The Inhibition of N_2O_5 Hydrolysis in Sulfuric Acid by 1-Butanol and 1-Hexanol Surfactant Coatings

Seong-Chan Park, Daniel K. Burden, and Gilbert M. Nathanson*

Department of Chemistry, University of Wisconsin−Madison, 1101 University Avenue, Madison, Wisconsin 53706

Received: November 30, 2006; In Final Form: February 16, 2007

Gas−liquid scattering experiments are used to measure the fraction of N_2O_5 molecules that are converted to HNO_3 after colliding with 72 wt % H_2SO_4 containing 1-hexanol or 1-butanol at 216 K. These alcohols segregate to the surface of the acid, with saturation coverages estimated to be 60% of a close-packed monolayer for 1-hexanol and 44% of a close-packed monolayer for 1-butanol. We find that the alkyl films reduce the conversion of N_2O_5 to HNO_3 from 0.15 on bare acid to 0.06 on the hexyl-coated acid and to 0.10 on the butyl-coated acid. The entry of HCl and HBr, however, is enhanced by the hexanol and butanol films. The hydrolysis of N_2O_5 may be inhibited because the alkyl chains restrict the transport of this large molecule and because the alcohol OH groups dilute the surface region, suppressing reaction between N_2O_5 and near-interfacial H_3O^+ or H_2O. In contrast, the interfacial alcohol OH groups provide additional binding sites for HCl and HBr and help initiate ionization. These and previous scattering experiments indicate that short-chain alcohol surfactants impede or enhance sulfuric acid-mediated reactions in ways that depend on the chain length, liquid phase acidity, and nature of the gas molecule.

Introduction

The aerosol-mediated conversion of N_2O_5 into HNO_3 is a key step in regulating ozone levels in the stratosphere and troposphere and in denitrifying the troposphere through wet and dry deposition of nitric acid.[1−6] Because N_2O_5 is formed at night from NO_2 and NO_3 and photolyzes back into these species during the day, the reaction

$$N_2O_5 + H_2O \xrightarrow{\text{aerosol}} 2HNO_3 \qquad (1)$$

effectively converts NO_2 and NO_3 into the temporary reservoir species HNO_3. In the lower stratosphere, this reaction suppresses the NO/NO_2-catalyzed destruction of ozone while enhancing both the HO/HO_2 cycle (through photolysis of HNO_3 into OH and NO_2) and the Cl/ClO cycle (by curtailing formation of $ClONO_2$) that reduce O_3.[7] Inclusion of this hydrolysis reaction in models of the lower stratosphere and upper troposphere lead to better agreement between predicted and observed O_3 depletion rates and ratios of nitrogen oxide species.[8,9] In the global troposphere, N_2O_5 hydrolysis occurs on a variety of aqueous surfaces[10] and is estimated to reduce NO and NO_2 levels by ∼40% and O_3 levels by ∼5% during winter months.[11−13]

The hydrolysis of N_2O_5 is typically mediated by submicron sulfuric acid particles in the lower stratosphere that range from 40 to 80 wt % H_2SO_4 at temperatures from 200 to 240 K, with wider variations in acidity in the upper troposphere due to absorption of NH_3.[3,4] Laboratory studies demonstrate that N_2O_5 hydrolysis occurs with a probability near 0.1 in sulfuric acid aerosols over a wide range of acid concentrations at low temperatures.[14−19] Field measurements indicate that, in the upper troposphere and tropopause regions, these aerosol particles contain significant concentrations of organic species.[20] Neither the abundance nor the speciation of these organic molecules is firmly established, but they are expected to range from small molecules such as methanol and acetone to long-chain fatty acids.[21−24] These molecules may segregate to the surface of the acid droplets and coat them, potentially impeding interfacial transport and suppressing N_2O_5 hydrolysis. Organic coatings have been recently suggested to be one explanation for the variability in N_2O_5 hydrolysis rates on acidic particles over the northeast United States.[25] In this article, we focus on the effects of two soluble alcohols, 1-butanol and 1-hexanol, on N_2O_5 hydrolysis in 72 wt % H_2SO_4 at 216 K and compare hydrolysis rates with HCl and HBr uptake into the bare and film-coated acids.

Insoluble and soluble organic species behave very differently at the surfaces of aqueous solutions. Numerous experiments show that insoluble, long-chain surfactants such as hexadecanol ($C_{16}H_{33}OH$) form compact monolayers on water and sulfuric acid that inhibit rates of water evaporation by 10^4 or more, with resistances that grow exponentially with chain length.[26] Kinks in the chain moderate this resistance substantially, as demonstrated recently by the 10-fold greater permeation of acetic acid through films of *cis*-9-octadecen-1-ol ($C_{18}H_{36}O$) on water than through the straight-chain 1-octadecanol.[27] Permeation data are scarce for short-chain surfactants: slightly soluble C_8−C_{12} alcohols in water may impede H_2O and CO_2 transport,[28] and organic films can even enhance uptake when the gas is more soluble in the surface film than in the subphase, as shown by the adsorption of anthracene onto 1-octanol-coated water.[29] Conversely, recent fluorescence experiments indicate that 1-octanol films on water suppress interfacial pH changes induced by exposure to HNO_3 or NH_3.[30]

Most pertinent to the present study are experiments by Thornton and Abbatt, which demonstrate that a monolayer of hexanoic acid on synthetic seawater aerosol reduces N_2O_5 hydrolysis by 3- to 4-fold.[31] Further experiments by McNeill

* To whom correspondence should be addressed. E-mail: Nathanson@chem.wisc.edu.

10.1021/jp068228h CCC: $37.00
Published on Web 03/24/2007

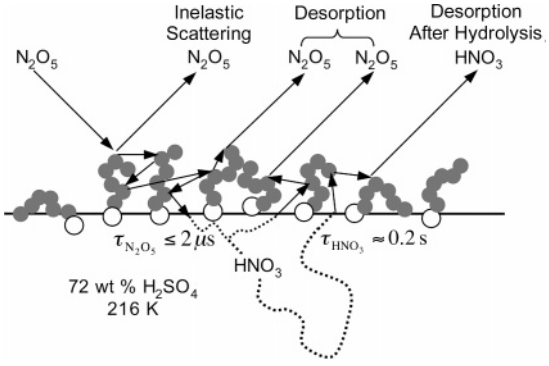

Figure 1. Several pathways for an N_2O_5 molecule colliding into sulfuric acid containing 1-hexanol. The τ values refer to the average liquid-phase residence times of unreacted N_2O_5 and HNO_3.

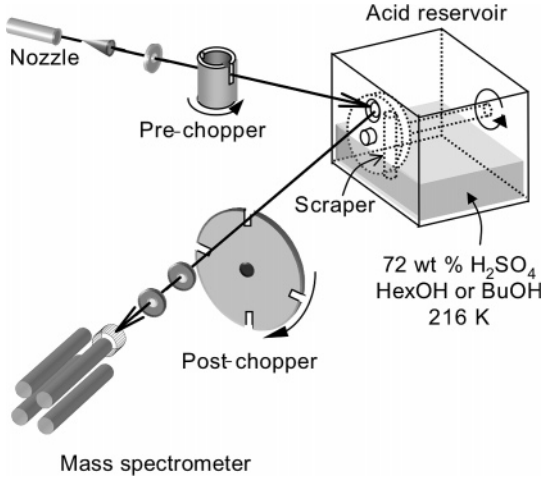

Figure 2. Molecular beam scattering apparatus and liquid reservoir. The Teflon reservoir is sealed except for a 0.9 cm diameter hole through which the N_2O_5 beam strikes the acid. Only one of the prechopper or postchopper wheels is used at one time.

et al. show that sodium dodecyl sulfate coatings on natural seawater and NaCl aerosols reduce hydrolysis of N_2O_5 10-fold.[32] Folkers et al. and Anttila et al. also showed that aqueous sulfate particles coated with thick, multilayer films formed from monoterpene oxidation reduce N_2O_5 hydrolysis by factors of 10 or more.[33,34]

N_2O_5 molecules can follow a range of pathways upon collision with a submonolayer organic film on sulfuric acid, as illustrated in Figure 1 for acid coated with hexanol molecules in different chain conformations.[35,36] At thermal collision energies, nearly all impinging N_2O_5 molecules will be momentarily trapped at the surface, and only a small fraction will recoil directly (inelastic scattering).[37,38] Some of the thermalized N_2O_5 may then desorb from the surface before or after moving between the hexyl chains, while others may permeate through the porous film and undergo hydrolysis near the film−acid interface or deeper into the acid.

Our previous studies of butanol and hexanol coatings on 56 to 68 wt % D_2SO_4 (0.20 to 0.30 mole fraction acid) at 213 K led us to suspect that these films would not significantly inhibit N_2O_5 passage into the acid because they do not form compact monolayers.[37−40] Each alcohol reacts with H_2SO_4 to form mixtures of ROH, ROH_2^+, $ROSO_3^-$, and $ROSO_3H$, which are expected to be in roughly equal proportions in 70 wt % H_2SO_4 at 298 K.[41] On the basis of surface tension measurements of 72 wt % H_2SO_4 mixed with butanol and hexanol at 295 and 250 K, the total surface concentration of all alkyl species at 216 K is predicted to saturate at $\sim 3.0 \times 10^{14}$ cm^{-2} (~60% of a close-packed monolayer) for 1-hexanol and $\sim 2.2 \times 10^{14}$ cm^{-2} (~44% of a close-packed monolayer) for 1-butanol.[38] Our first studies indicated that butyl films on 56−68 wt % D_2SO_4 at 213 K do not impede water evaporation and actually enhance HCl and HBr uptake by providing extra OH surface groups that act as protonation sites for HCl and HBr dissociation.[37,39] When hexanol is substituted for butanol, the entry of HCl is still enhanced, except when the acid concentration is low enough (56 wt % D_2SO_4) to reduce the fraction of $HexOH_2^+$ and allow the hexyl film coverage to rise to ~68% of a compact monolayer.[38] At this higher packing, HCl uptake is reduced from 0.68 to 0.59 and water evaporation is reduced by 20%. In contrast to the enhanced uptake of HCl and HBr by the alcohol films, the uptake of the basic molecule CF_3CH_2OH is nearly 1 at all acid concentrations and is impeded by less than 4% by both butyl and hexyl films.

The observations above indicate that gas transport through surface films is controlled by the chain length of the surfactant, the identity of the gas molecule, and the underlying liquid. Hexanol and butanol films on sulfuric acid may therefore alter N_2O_5 hydrolysis differently than HCl and HBr uptake, and they may act differently on sulfuric acid or other subphases. The experiments below utilize 72 wt % H_2SO_4 or 70 wt % D_2SO_4 at 216 K, each 0.32 mole fraction acid, which are highly viscous (~1900 cP) and low vapor pressure ($\sim 2 \times 10^{-4}$ Torr) liquids.[42,43] They show that, although the hexyl and butyl films significantly enhance HCl and HBr uptake, the conversion of N_2O_5 to HNO_3 drops by 60% and 33%, respectively, indicating that submonolayer films can impede this near-surface reaction.

Experimental Procedure

N_2O_5 and Acid Preparation. N_2O_5 is synthesized by oxidizing NO with O_2 and O_3 consecutively at room temperature, purifying the product by distillation under O_3 and storing it at 195 K.[44] HNO_3 formation is minimized by baking the apparatus and by passing NO and dried O_2 through a 195 K cold trap to remove H_2O. The melting point of the N_2O_5 sample under argon was observed to be 39−42 °C, which encompasses the literature value of 41 °C.[45] During the scattering experiments, the sample is held at 253 K, where the N_2O_5 vapor pressure is estimated to be 8 Torr.[46] Incident beams of 13 and 150 kJ mol^{-1} N_2O_5 are created by expanding pure N_2O_5 or N_2O_5 seeded in 750 Torr H_2 through an unheated, 0.13 mm diameter glass nozzle.

Surfactant/acid solutions are prepared by diluting 97 wt % H_2SO_4 to 72 wt % with Millipore water, adding 1-hexanol (up to 0.1 M) or 1-butanol (up to 1 M) and immediately cooling to 216 ± 0.5 K in the liquid reservoir shown in Figure 2. The alcohols (Aldrich, >99% pure) are used without further purification. Titrations indicate that the acid concentration changes by no more than 0.5 wt % during the time it is in vacuum (typically less than 3 days). The measured reductions in surface tension upon adding alcohol are those expected when adding soluble, small-molecule surfactants, indicating that the alcohols are not contaminated with long-chain insoluble species.[40]

A continuously renewed, vertical liquid film is formed by rotation of a 5.0 cm diameter glass wheel partially submerged in 60 mL of the acid solution.[39] The acid-coated wheel is skimmed by a cylindrical Teflon scraper, which removes the outer 0.1 cm of acid and alcohol. The remaining ~0.03 cm thick acid film then passes in front of a 0.7 cm^2 circular hole, where it is intercepted by the N_2O_5 beam impinging at an incident

angle θ_{inc} of 45°. At a typical wheel speed of 0.17 Hz, the time interval between scraping and exposure to the beam is 0.49 s. Argon scattering measurements show that this time is sufficient to allow the butyl and hexyl films to become reestablished at the surface of the acid, as shown previously in refs 38 and 39. The acid remains in front of the hole in the reservoir for 0.45 s and is exposed to the incident beam for a time t_{exp} equal to 0.27 s.

Distinguishing N_2O_5 and HNO_3 by Pre- and Postchopper TOF Analysis. Time-of-flight (TOF) spectra of N_2O_5 and HNO_3 exiting from the acid are recorded by a differentially pumped quadrupole mass spectrometer oriented at an angle $\theta_{fin} = 45°$, as shown in Figure 2. Electron-impact ionization is used to detect the neutral molecules with an electron energy of 70 eV. Unfortunately, the $N_2O_5^+$ parent ion is unstable and all stable N_2O_5 ion fragments are also produced by HNO_3 ionization. Here we monitor the most abundant fragment, NO_2^+ ($m/z = 46$), and employ pre- and postchopper TOF analysis to distinguish N_2O_5 and HNO_3 by their short ($<10^{-6}$ s) and long ($\sim$0.1 to 10 s) residence times, respectively, in the acid. The pre- and postchopper wheels are shown in Figure 2. With the postchopper wheel in place and the prechopper wheel removed, the incident beam strikes the liquid continuously and the exiting molecules are chopped into 36 μs pulses upon exiting the acid. The arrival times of these molecules at the mass spectrometer in the postchopper spectrum therefore depend only on the velocities of the exiting molecules. In contrast, the prechopper wheel slices the incident beam into 50 μs pulses, and the total arrival time at the mass spectrometer in the prechopper spectrum depends on the residence times of the molecules in the acid solution as well as their gas-phase flight times. As described below, the HNO_3 signal can be obtained by subtracting the prechopper spectrum (containing only N_2O_5) from the postchopper spectrum (containing both N_2O_5 and HNO_3).

The raw TOF signals are converted into relative N_2O_5 and HNO_3 signals by correcting for the different ionization cross sections $\sigma_{NO_2^+}$ for dissociative ionization of N_2O_5 and HNO_3 into NO_2^+. These cross-sections were calculated by multiplying the total ionization cross section σ_{tot} of each parent molecule by the branching ratio r for NO_2^+ formation. We used the following values to calculate $\sigma_{NO_2^+}$: σ_{tot} (N_2O_5) = 7.0 Å^2 from ref 47, r ($N_2O_5 \rightarrow NO_2^+$) = 0.54 from ref 48, σ_{tot} (HNO_3) = 6.3 Å^2 from ref 49, and r ($HNO_3 \rightarrow NO_2^+$) = 0.60 from ref 50. Each value is measured at an electron energy of 70 eV, which is equal to our experimental setting. Fortuitously, $\sigma_{NO_2^+}$ is 3.8 Å^2 for both N_2O_5 and for HNO_3. The relative intensities of HNO_3 and N_2O_5 are therefore equal to the relative fluxes obtained from the TOF spectra to within an estimated uncertainty of ±15% in the ionization parameters. This systematic uncertainty is not included in the error bars reported for the hydrolysis probabilities because $\sigma_{NO_2^+}$ does not change the ratio of probabilities for the bare and alcohol-coated acids.

Monitoring HNO_3 Desorption. The mass spectrometer is collimated to monitor a patch of the acid-coated wheel for a time equal to the exposure time, t_{exp}, of 0.27 s. This observation time is insufficient to observe the complete evaporation of the HNO_3 product, which desorbs over several seconds because of its high solubility of 2×10^6 M atm^{-1} in 72 wt % H_2SO_4 at 216 K (as described in the Appendix). To monitor most of the HNO_3 desorption, the wheel is periodically stopped for 6 s and the HNO_3 desorption signal is recorded. The liquid is viscous enough (1900 cP at 216 K) that it sags only slightly during this stop period; a droop in the acid film does not distort the measurements because the hydrolysis probability is determined from a *ratio* of pre- and postchopper signals, as shown later in eq 2. The reliability of this start−stop procedure has been tested in three ways: (1) high-energy argon scattering from the stopped wheel (t_{exp} = 6 s) and continuously moving wheels (t_{exp} = 0.27 s) are identical, implying that the packing of the butyl and hexyl films remains the same on the stationary and moving films,[38,39] (2) measurements of the HBr → DBr and HCl → DCl exchange fractions (ranging from 0.08 to 0.60) in D_2SO_4 using the stopped wheel differ by less than ±0.02 from measurements using a continuously moving wheel, and (3) the N_2O_5 hydrolysis probabilities in bare 72 wt % H_2SO_4 when measured from the stopped wheel and from the moving wheel are each 0.15 ± 0.02 after correcting for the fraction of HNO_3 remaining in the acid, as described in the Appendix.

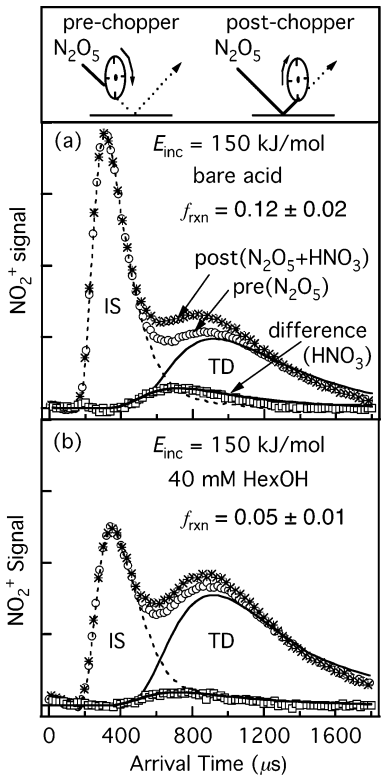

Figure 3. Pre- and postchopper TOF spectra of N_2O_5 and their difference spectra following collisions of 150 kJ mol^{-1} N_2O_5 with 72 wt % H_2SO_4 containing (a) no hexanol and (b) 40 mM hexanol. The difference spectra correspond to thermal desorption of HNO_3 molecules generated by N_2O_5 hydrolysis. N_2O_5 inelastic scattering (IS) is fit by a dotted curve. The difference spectra and the thermal desorption (TD) component of the N_2O_5 prechopper spectra are fit by Maxwell−Boltzmann distributions shown with solid curves.

Hexanol Solubility Measurements. The solubility of hexanol in 72 wt % H_2SO_4 was measured by comparing hexanol mass spectrometer signals from pure hexanol (of known vapor pressure[51]) and from 0.02 to 0.1 M hexanol in the acid at 253, 243, and 233 K. The vapor pressures varied linearly with hexanol concentration, and when extrapolated to 216 K, yield a hexanol solubility of $3.2 \pm 0.4 \times 10^8$ M atm^{-1} and an enthalpy of vaporization of 78 ± 2 kJ mol^{-1}. As discussed later, the solubility of butanol is expected to be slightly lower.[52]

Results and Analysis

Hydrolysis of N_2O_5 by Bare Sulfuric Acid. Figure 3a compares pre- and postchopper TOF spectra recorded at m/z = 46 (NO_2^+) following collisions of 150 kJ mol^{-1} N_2O_5 with uncoated 72 wt % H_2SO_4 at 216 K. In the postchopper mode, the arrival time distribution depends only on the velocities of

TABLE 1: N_2O_5 Hydrolysis Probabilities and HCl and HBr HX → DX Exchange Fractions Measured for 72 wt % H_2SO_4 or 70 wt % D_2SO_4 at 216 K

acid solution	N_2O_5 f_{rxn} (eq 2)[a]	N_2O_5 hydrolysis probability γ[b]	HCl → DCl exchange fraction[c]	HBr → DBr exchange fraction[c]
bare acid	0.12 ± 0.02	0.15 ± 0.02	0.08 ± 0.03	0.19 ± 0.02
180 mM BuOH	0.08 ± 0.02	0.10 ± 0.02	0.20 ± 0.02	0.63 ± 0.02
40 mM HexOH	0.05 ± 0.01	0.06 ± 0.01	0.16 ± 0.02	0.60 ± 0.02

[a] Measured in both 70 wt % D_2SO_4 and 72 wt % H_2SO_4, each 0.32 mole fraction acid. [b] The hydrolysis probability γ is obtained from f_{rxn} after using eq A.1 to correct for HNO_3 molecules accumulating in solution and assuming no production of alkyl nitrates. [c] Measured in D_2SO_4 by H → D exchange. These values are equated with the entry probability of HX, either as molecular HX or as X^- and H^+/D^+.[38]

the exiting N_2O_5 and HNO_3 molecules. Therefore, both species contribute to the TOF spectra measured at $m/z = 46$, regardless of their residence times in the acid. In the prechopper mode, the TOF spectrum is a convolution of the gas-phase velocities of the molecules and their residences times in the acid. The average residence time of HNO_3 is so long (~0.2 s), and the residence times of the individual molecules are so broadly distributed, that the desorption times of the exiting HNO_3 molecules are not correlated with the incident pulses. In this case, the HNO_3 desorption signal merges with the background. This was shown previously in Figure 3 of ref 53 for collisions of HNO_3 with 70 wt % D_2SO_4 at 213 K. As described later, the residence time of N_2O_5 lies in the opposite limit; it is shorter than the minimum 10^{-6} s residence time that visibly alters the prechopper TOF spectrum.[38,53] Therefore, the prechopper spectra measured at $m/z = 46$ in Figure 3a is composed only of unreacted N_2O_5 molecules and is equivalent to the postchopper spectra of N_2O_5. By subtracting the prechopper spectrum containing only N_2O_5 signal from the postchopper spectrum with contributions from both N_2O_5 and HNO_3 signals, we obtain the postchopper TOF spectrum of HNO_3.

The bimodal feature of the prechopper spectrum in Figure 3a reveals that N_2O_5 molecules with high incidence energy follow two distinct pathways upon colliding with the surface, as depicted in Figure 1. The narrow, inelastic scattering (IS) peak at early arrival times (high exit velocities) corresponds to molecules that recoil directly from the surface, transferring a portion of their kinetic energy through one or a few bounces. The broader peak at later arrival times (lower exit velocities) arises from N_2O_5 molecules that become thermalized through dissipation of their excess energy and then thermally desorb (TD). This prechopper TD component is fit well by a Maxwell−Boltzmann (MB) distribution at the acid temperature of 216 K with a mass of N_2O_5 (108 amu) and the difference spectrum is fit well by an MB curve with a mass of HNO_3 (63 amu), supporting our experimental approach to identifying them.

The difference spectrum corresponds to thermalized N_2O_5 molecules that undergo hydrolysis and then desorb as HNO_3, while the prechopper TD signal represents the remaining N_2O_5 molecules that thermally desorb before converting to HNO_3. Therefore, the fraction f_{rxn} of the thermalized N_2O_5 molecules that are converted into HNO_3 is calculated from

$$f_{rxn} = \frac{{}^1/_2 I_{TD}^{HNO_3}}{I_{TD}^{N_2O_5} + {}^1/_2 I_{TD}^{HNO_3}} \approx \frac{{}^1/_2 I_{TD}^{diff}}{I_{TD}^{pre} + {}^1/_2 I_{TD}^{diff}} \qquad (2)$$

where $I_{TD}^{pre}(I_{TD}^{N_2O_5})$ and $I_{TD}^{diff}(I_{TD}^{HNO_3})$ are the relative fluxes of thermally desorbing molecules of the prechopper (N_2O_5) and the difference (HNO_3) TOF spectra, respectively. The factor of $^1/_2$ in eq 2 arises from the stoichiometry of eq 1. The measured exchange fraction from Figure 3a is 0.12 ± 0.02. The ± 0.02 error bar reflects one standard deviation in reproducibility of ±0.01 and an estimated ±0.01 uncertainty in fitting the TD component. Finally, f_{rxn} must be corrected for those HNO_3 molecules that accumulate within the acid and do not desorb over the 6 s observation time. This correction, described in the Appendix, shows that 18% of the HNO_3 remain behind and therefore that I_{TD}^{diff} must be replaced by $I_{TD}^{diff}/0.82$. The corrected hydrolysis probability γ is then found to be 0.15 ± 0.02, as summarized in Table 1.

Hydrolysis of N_2O_5 by Hexyl-Coated Sulfuric Acid. The effects of doping the 72 wt % H_2SO_4 solution with 40 mM hexanol are displayed in Figure 3b. Surface tension measurements indicate that, at this hexanol bulk concentration, the hexyl surface concentration reaches its saturation value of 3.0×10^{14} cm^{-2}, corresponding to 60% of a compact monolayer.[38,54] Upon addition of hexanol, the N_2O_5 direct scattering channel decreases and the total (N_2O_5 + HNO_3) desorption channel increases. These trends have been observed before in hyperthermal collisions of Ar, HCl, and HBr with sulfuric acid containing hexanol or butanol; they occur because the alkyl groups roughen the surface and reduce its effective mass, increasing the likelihood that N_2O_5 will thermalize upon collision.[38,39]

The most important change in Figure 3b is seen in the value of f_{rxn}, which drops from 0.12 ± 0.02 to 0.05 ± 0.01 upon addition of hexanol. This reduction may be caused by at least three different factors: (1) a reduced hydrolysis efficiency imposed by the surface hexyl film, (2) a reduction in the HNO_3 desorption flux because the hexyl film increases the HNO_3 residence time in the acid, and (3) reaction of N_2O_5 or HNO_3 with the hexyl species to produce hexyl nitrate. We examined the effect of added hexanol on the average HNO_3 residence time by measuring HNO_3 desorption at two different observation times of 0.27 and 6 s. These times were selected by continuously spinning the acid-coated wheel at 0.17 Hz and by stopping the wheel, respectively. As shown in Figure 4a and b, fewer HNO_3 molecules desorb over the 0.27 s observation time than over the 6 s period for both bare and hexyl-coated acids. The ratios of 0.60 (bare acid) and 0.63 (hexyl-coated acid) are identical to within our uncertainty, indicating that the hexyl film does not measurably impede evaporation of HNO_3.

Hexyl species at the surface or in the acid may also react directly with N_2O_5 or with HNO_3 generated by hydrolysis to produce hexyl nitrate, $CH_3(CH_2)_5ONO_2$, according to the reactions ROH + N_2O_5 → $RONO_2$ + HNO_3 and ROH + HNO_3 → $RONO_2$ + H_2O. Hexyl nitrate should, like hexanol itself, evaporate slowly from solution, with dominant cracks in the mass spectrometer at $m/z = 46$, co-incident with NO_2^+, at $m/z = 43$, which does not overlap with N_2O_5 or HNO_3 but does overlap with hexanol, and at $m/z = 76$, which is unique to hexyl nitrate. Repeated searches at each m/z value showed no evidence of a signal that could be assigned to the alkyl nitrate. We conservatively estimate that the uncertainty in these searches is ~5% of the total HNO_3 signal. The ratio of ionization cross sections at NO_2^+ for hexyl nitrate and nitric acid is expected to be ~$^1/_3$, based on the cracking patterns of each molecule[50,55]

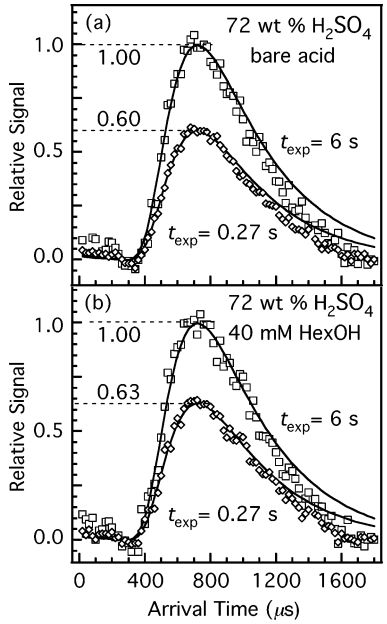

Figure 4. HNO_3 difference spectra obtained at two beam exposure times, $t_{exp} = 0.27$ s (◇) and 6 s (□), following collisions of 150 kJ mol^{-1} N_2O_5 with 72 wt % H_2SO_4 containing (a) no hexanol and (b) 40 mM hexanol. In each panel, the TOF signals are normalized to the signal at $t_{exp} = 6$ s.

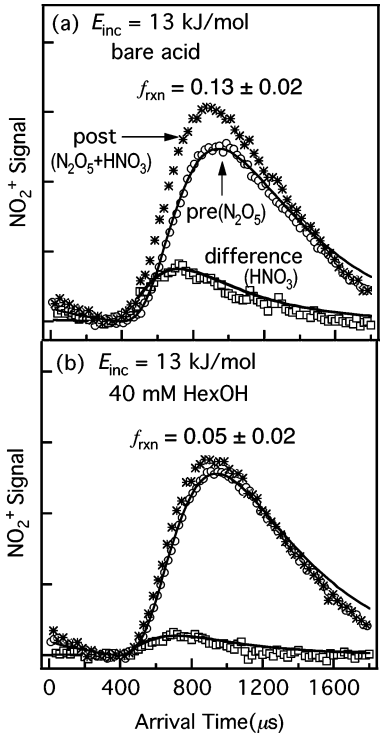

Figure 5. Pre- and postchopper TOF spectra of N_2O_5 and the difference spectra following collisions of N_2O_5 at a low incidence energy of 13 kJ mol^{-1} with 72 wt % H_2SO_4 containing (a) no hexanol and (b) 40 mM hexanol.

and assuming that the total ionization cross sections scale with the number of electrons in each molecule.[49] The relative TOF signals N may then be converted to relative fluxes $I = N\langle v \rangle$ by multiplying by the ratio of their average velocities, which is $\langle v_{\text{hexyl nitrate}} \rangle / \langle v_{\text{nitric acid}} \rangle = 0.7$. These numbers imply that the fraction of hexyl nitrate produced should not exceed $3 \times 0.7 \times 0.05 \approx 0.1$ of the HNO_3 flux. Thus, the formation of hexyl nitrate may be as high as 10% of the formation of HNO_3, increasing the total loss of N_2O_5 into the hexyl-coated acid from 0.05 to 0.055, a difference that lies within the precision of the measurement. This adjustment is not incorporated into the analysis below, but it remains a source of uncertainty in our experiments. In the absence of this nitration channel, we conclude that the reduction in HNO_3 desorption imposed by the hexyl film is due to a reduction in the hydrolysis of N_2O_5.

The TOF spectra in Figures 3 and 4 were generated by collisions of N_2O_5 at an incident energy of 150 kJ mol^{-1} (84 RT_{liq}), chosen because this high energy beam has a high flux (estimated to be 6×10^{14} cm^{-2} s^{-1} or approximately one monolayer s^{-1}) and because the IS and TD components are well separated at this energy. To determine if this high collision energy skews the value of f_{rxn}, experiments were performed at the much lower incident energy of 13 kJ mol^{-1} (7 RT_{liq}), where the N_2O_5 flux is reduced by half. As shown in Figure 5, nearly all impinging N_2O_5 molecules thermalize on the surface, and no IS channel can be discerned in the pre- or postchopper spectra. The measured f_{rxn} value of 0.05 ± 0.02 matches the value of 0.05 ± 0.01 found at high incident energy in Figure 3. The invariance of f_{rxn} with incidence energy implies that f_{rxn} may be considered to be a measurement of the hydrolysis probability γ that is conventionally reported for thermal-energy collisions at $2RT_{acid} = 3.6$ kJ mol^{-1} (neglecting any production of hexyl nitrate). As described in the Appendix, these values must be corrected for HNO_3 that remains behind in solution. The corrected values are listed in the third column of Table 1, which are just slightly higher than f_{rxn}. The observed reduction in the hydrolysis probability γ from 0.15 to 0.06 reveals that the addition of 40 mM hexanol to 72 wt % H_2SO_4 decreases γ by more than half.

Figure 6a displays the dependence of f_{rxn} on the bulk-phase concentration of hexanol in 72 wt % H_2SO_4 at 216 K. The open circles represent the surface concentration of hexyl species calculated from surface tension measurements for 72 wt % H_2SO_4 at 295 K.[54] This coverage follows a Langmuir-type adsorption curve, rising rapidly at low-bulk hexanol concentrations and then plateauing near 20 mM. The production of HNO_3 follows an opposite trend: f_{rxn} decreases sharply and then also plateaus. The correlation between f_{rxn} and hexyl surface coverage implies that the reduction in hydrolysis with the addition of hexanol is caused by the presence of hexyl species that segregate at the surface rather than by hexyl species dissolved in the bulk.

Hydrolysis of N_2O_5 by Butyl-Coated Sulfuric Acid. We also investigated changes in N_2O_5 hydrolysis upon adding 1-butanol, a soluble surfactant that is two CH_2 groups shorter than 1-hexanol. Figure 6b plots f_{rxn} against the bulk concentration of butanol following collisions of 160 kJ mol^{-1} N_2O_5 with 72 wt % H_2SO_4 at 216 K. The value of f_{rxn} drops from 0.12 ± 0.02 for bare acid to 0.08 ± 0.02 for 180 mM butanol (44% of a compact monolayer) and then does not change significantly with further increasing butanol bulk concentration. As shown in Table 1, the hydrolysis probabilities γ corrected for residual HNO_3 in the acid are 0.15 (bare acid) and 0.10 (180 mM butanol). Just as with hexanol in panel a, the trend in f_{rxn} is opposite to that of the surface segregation of butyl species (open circles).

The data in panels a and b may be used to plot $\gamma_{film}/\gamma_{bare}$ directly against the surface coverage θ_{film} in panel c, where $\theta_{film} = n_{surf}/n_{max}$ is the fraction of a compact monolayer covered by the film and n_{max} is $\sim 5 \times 10^{14}$ cm^{-2} in the close-packed configuration.[56] The surface concentrations n_{surf} were obtained from the surface tension measurements at 295 and 250 K and linearly extrapolated to 216 K.[39,54] Panel c indicates that N_2O_5

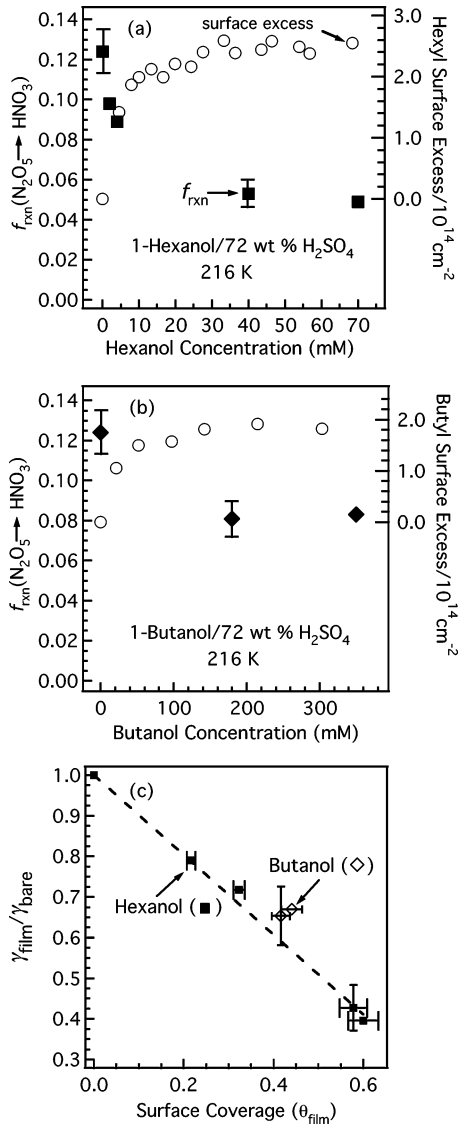

Figure 6. Fraction f_{rxn} of N_2O_5 converted to HNO_3 vs (a) hexanol and (b) butanol bulk concentration in 72 wt % H_2SO_4 at 216 K. The hexyl and butyl surface concentrations at 295 K are plotted against the right-hand axis as open circles. The error bars represent $\pm 1\sigma$ for 5 measurements (bare acid), 3 (40 mM hexanol), and 3 (180 mM butanol). The other points represent single measurements. (c) The ratio of hydrolysis probabilities $\gamma_{film}/\gamma_{bare}$ vs fractional surface coverage θ_{film} from the data in panels a and b and the Appendix. The θ_{film} values were obtained from surface tension data at 295 and 250 K and extrapolated to 216 K.[54] The dashed line is a fit to the hexanol data.

hydrolysis decreases approximately linearly with hexanol surface coverage, such that $\gamma_{hexyl}/\gamma_{bare} = 1 - m\theta_{hexyl}$ with $m = 1.0 \pm 0.2$ (dashed line). The single cluster of butanol values, combined with the uncertainty in determining θ_{film}, makes it difficult to determine if the shorter-chain alcohol impedes hydrolysis less effectively at constant surface coverage.

Collisions of HCl and HBr with Hexyl-and Butyl-Coated Sulfuric Acid. To gauge the effects of hexyl and butyl films on HCl and HBr uptake into the acid, we also measured the extent of HX → DX exchange following collisions of 100 kJ mol^{-1} HCl and 150 kJ mol^{-1} HBr from 70 wt % D_2SO_4 at 216 K containing no surfactant, 40 mM hexanol, and 180 mM butanol. As discussed in refs 37, 38, and 53, the fraction f_{exch} of thermalized HX molecules that undergo D → H exchange can be interpreted as the entry probability of HCl and HBr into the acid, either as molecular HX or as X^- and H^+ following dissociation at the surface. Table 1 shows that, in contrast to N_2O_5 hydrolysis, HCl and HBr entry is significantly enhanced by the surface films.

Discussion

It is striking that the butyl and hexyl films on 72 wt % H_2SO_4 at 216 K impede N_2O_5 hydrolysis because these same films enhance HCl and HBr uptake into 70.2 wt % D_2SO_4, as shown in Table 1. H/D isotope effects are not responsible for the different outcomes; the same reduction in N_2O_5 hydrolysis by the hexyl film is observed using 70 wt % D_2SO_4 and 72 wt % H_2SO_4, which are each 0.32 mole fraction acid.

Previous studies in our laboratory suggest that the entry of HCl and HBr into D_2SO_4/D_2O solutions containing hexanol at 213 K is controlled by two competing effects: hexyl chains at the surface impede gas transport through the film, while the basic hexanol OD groups assist HX entry by providing extra surface sites for HCl and HBr dissociation.[38] As the underlying solution is made more acidic, the hexyl and butyl films become more porous and HCl and HBr molecules can more easily reach the alcohol OD groups and protonate them. In particular, a saturated hexyl film on 68 wt % D_2SO_4, which corresponds to 62% coverage of a compact monolayer, enhances the entry of HCl from 0.14 (bare acid) to 0.23 and of HBr from 0.29 to 0.63, whereas a saturated hexyl film on 56 wt % acid, corresponding to 68% coverage, reduces HCl entry from 0.69 to 0.58. N_2O_5 lacks the acidic proton of HCl and HBr and cannot follow this pathway. In 70 wt % H_2SO_4 at cold temperatures, N_2O_5 hydrolysis is postulated to proceed primarily through an acid-catalyzed channel consisting of $N_2O_5 + H^+ \rightarrow HNO_3 + NO_2^+$ and $NO_2^+ + H_2O \rightarrow HNO_3 + H^+$.[17,57] The surface alcohol OH and OH_2^+ groups could potentially substitute for H_2O and H^+ as reactants and convert N_2O_5 into HNO_3 and alkyl nitrate. The reduction in N_2O_5 hydrolysis we observe and the absence of a signal attributable to the alkyl nitrate indicate that these reactions do not readily occur and that the surface alcohol molecules instead impede the conversion of N_2O_5 to HNO_3.

This reduction in N_2O_5 hydrolysis may be framed within two scenarios motivated by the steady decrease in the fractional hydrolysis rate $\gamma_{hexyl}/\gamma_{bare}$ with hexanol surface coverage θ_{hexyl} shown in Figure 6c: (1) the hexyl chains block entry of N_2O_5 into the acid, and (2) the hexyl head groups reduce the hydrolysis rate in the near-interfacial region. The steady decrease in Figure 6c is described by the relation $\gamma_{hexyl}/\gamma_{bare} \approx 1 - (1 \pm 0.2)\theta_{hexyl}$ over the range of $\theta_{hexyl} = 0$ to 0.6, where θ_{hexyl} is the fraction of the surface area covered by hexyl chains in the all-trans configuration (~20 Å^2 in area and ~10 Å long).[56,58] Clifford et al. have recently observed, for 1-octanol films on water, that the interfacial hydrolysis of HNO_3 and NH_3 also decreases linearly with increasing film coverage.[30]

Within the first scenario, the passage of N_2O_5 into the acid is limited to motions though fluctuating gaps between the hexyl chains, which become less prevalent as more hexyl species segregate to the surface at higher bulk-phase concentration and become more tightly packed. These gaps arise because, at intermediate coverages, the hexyl chains should adopt a range of configurations with varying spacings and relative positions, as pictured in simulations of butanol and heptanol on water[35,36,39] and inferred from neutron reflection studies of hexanol on water[58] and sum frequency generation studies of hexanol on 59.5 wt % H_2SO_4.[59] The approximate scaling between $\gamma_{hexyl}/\gamma_{bare}$ and $1 - \theta_{hexyl}$ implies a constant "blocking power" for each added hexyl chain. This simple correlation may be accidental, however, because the various hexyl chain conformations project different surface areas and span different lengths,

and the range of these structures becomes more restricted as the chain density increases. In particular, this scaling will likely fail as θ approaches 1 and the chains become highly aligned and compact; for insoluble long-chain surfactants, gas permeation is observed to decrease exponentially with surface concentration at high coverage.[26]

The model above may be analyzed quantitatively in the limit that hydrolysis occurs far from the surfactant layer, which acts only to impede the entry of N_2O_5 into the acid. The hydrolysis probability may then be expressed as independent resistances using $1/\gamma_{hexyl} = 1/\alpha_{hexyl} + 1/\Gamma_{react}$, where α_{hexyl} is the probability that N_2O_5 passes through the hexyl film and enters the acid and Γ_{react} is the bulk-phase reactivity.[34,60,61] Γ_{react} does not vary upon addition of hexanol because hydrolysis occurs only within the bulk acid, where little hexanol is present. The range of values of Γ_{react} are obtained from $\gamma_{bare} = 0.15$ in Table 1 using the maximum value of $\alpha_{bare} = 1$ and its minimum value of 0.15, yielding $\Gamma_{react}(\alpha_{bare} = 1) = 0.18$ and $\Gamma_{react}(\alpha_{bare} = 0.15) = \infty$ (every entering molecule reacts). In the latter case when $\Gamma_{react} = \infty$, α_{hexyl} is equal to γ_{hexyl} and decreases linearly with θ_{hexyl}. When Γ_{react} is 0.18, α_{hexyl} starts at 1 for the bare surface and drops more sharply than γ_{hexyl}. At the highest surface coverage of $\theta_{hexyl} = 0.60$, the resistance equation predicts that α_{hexyl} varies between 0.09 ($\Gamma_{react} = 0.18$) and 0.06 ($\Gamma_{react} = \infty$). This analysis suggests that, if hydrolysis occurs far from the film region, then the saturated hexyl film must stop 90% or more of the thermalized N_2O_5 molecules from entering the acid.

The contrasting behaviors of N_2O_5 and HCl or HBr may be ascribed in part to their different sizes; the ~70 Å^3 molecular volume of N_2O_5 is approximately twice that of HCl and HBr, making it more difficult for N_2O_5 to pass through gaps between the alkyl chains. Thus, HCl and HBr may permeate more easily through the film and reach the underlying acid, where they can bond to and protonate the alcohol OH groups. Size arguments alone cannot justify a lower mobility of N_2O_5 through the film, however, because the molecular volumes of CF_3CH_2OH and N_2O_5 are very similar, but CF_3CH_2OH passes through the hexyl and butyl films on nearly every collision.[38] This difference points to a potentially critical role for solute OH groups in aiding transport within the porous film, perhaps via hydrogen bonds with H_2O, H_3O^+, or alcohol OH groups that straddle the film.[62]

We may also consider the opposite scenario in which N_2O_5, like CF_3CH_2OH, passes easily between the alkyl chains, but hydrolysis itself is suppressed by the interfacial alcohol species. Within this second picture, the $1 - \theta_{hexyl}$ behavior in Figure 6c reflects the role of the hexyl head groups, rather than the hexyl chains, in reducing the rate of reaction. Previous studies indicate that N_2O_5 hydrolysis in 70 wt % sulfuric acid is expected to occur very close to the surface.[16,17,63] In this region, the hexyl $-OH$ and $-OSO_3^-$ end groups may locally interfere with protonation of N_2O_5 by interfacial H_2SO_4 or H_3O^+, which is potentially the key step that initiates hydrolysis in acidic solutions.[17,57] In the limit in which hydrolysis occurs solely in the surface region and the hexyl film does not impede transport, the resistance equation reduces to $1/\gamma_{hexyl} \approx 1/S + 1/\Gamma_{surf}$ (where S, the trapping probability, approaches 1 at thermal collision energies, as shown in Figure 5).[60] In this case, Γ_{surf} scales approximately with γ_{hexyl} (for $\gamma_{hexyl} \leq 0.15$) and thus would be roughly proportional to $1 - \theta_{hexyl}$, which represents the fraction of surface area not covered by head groups.

Our experiments directly support the prediction that N_2O_5 hydrolysis takes place in a shallow layer near the surface, potentially in the vicinity of the hexyl or butyl species. According to continuum models,[17,60] the average depth over which a reaction occurs is equal to $(D/k)^{1/2}$, where D is the N_2O_5 diffusion coefficient and k is the hydrolysis rate constant. Reference 17 predicts that this depth is approximately 1 Å for 72 wt % H_2SO_4 at 216 K. In accord with this estimate, the thermal-desorption component of the prechopper TOF spectrum in Figures 4, 5, and 6 can be fit well with a Maxwell−Boltzmann distribution unconvoluted with a residence time distribution, indicating that the average bulk-phase residence time τ of intact N_2O_5 is less than 2×10^{-6} s.[53] In this case, the average diffusion depth of $0.6(D\tau)^{1/2}$ is less than 10 Å for $D \leq 10^{-8}$ cm^2 s^{-1}.[42,64] This experimental limit implies that hydrolysis often occurs in a region containing alcohol head groups and perhaps CH_2 groups as well.

The data in Figure 6 therefore suggest two possible causes for the suppression of N_2O_5 hydrolysis: the surface alkyl chains may pack tightly enough to block the entry of some N_2O_5 molecules into the acid, while the alcohol head groups may reduce the reactivity of N_2O_5 that do enter the acid, perhaps by reducing the concentration of both H_3O^+ and H_2O near the film−acid interfacial region.

Conclusions and Atmospheric Implications

Hexanol and butanol dissolved in 72 wt % H_2SO_4 at 216 K form loosely packed surface films corresponding to ~60% and ~44% of a compact monolayer at their asymptotic coverages, respectively. The conversion of N_2O_5 to HNO_3 is noticeably impeded by these surface films, with reaction probabilities that drop from 0.15 to 0.06 for the hexyl film and to 0.10 for the butyl film. These changes are smaller than those observed on seawater using hexanoic acid (3- to 4-fold reduction),[31] most likely because the alcohol films do not pack as tightly on acidic subphases due to charge repulsion among the ROH_2^+ head groups and formation of $ROSO_3^-$.[40,41]

The experiments demonstrate that short-chain alcohols can significantly impede N_2O_5 hydrolysis by sulfuric acid droplets if the alcohols are plentiful enough to form saturated surface films. However, it is unlikely that butanol and hexanol are present in the background upper troposphere or lower stratosphere to reach significant surface coverages. The two shortest alcohols, methanol and ethanol, have been identified at concentrations of ~1000 ppt and ~50 ppt (parts per trillion by volume), respectively, in polluted regions of the upper pacific troposphere at 10−12 km.[23,65] Our measured solubility of hexanol in 72 wt % H_2SO_4 at 216 K of 3×10^8 M atm^{-1} permits an estimate of the gas-phase concentration required to create a saturated hexyl film. For a typical pressure of 160 Torr at an altitude of 12 km, we estimate that the ~40 mM hexanol bulk concentration for a saturated hexyl film requires ~600 ppt of gas-phase hexanol. The solubility of butanol should lie between the hexanol value and that of ethanol of 2×10^8 M atm^{-1};[52] in this case, the ~200 mM butanol concentration for a saturated butyl film requires ~4000 ppt of gas phase butanol.

These minimum gas-phase concentrations rise rapidly in more dilute sulfuric acid because of lower alcohol solubilities. For 60 wt % H_2SO_4 at 216 K, which is closer to aerosol acidities near the tropopause region,[9] the solubility of the alcohols is expected to be near $\sim 4 \times 10^6$ M atm^{-1}.[52] This lower solubility requires the gas-phase hexanol concentration to increase to an even more improbable value of 50 000 ppt to create a saturated surface film. Butanol and hexanol alone are therefore not sufficiently surface active in sulfuric acid in the upper troposphere or lower stratosphere to impose barriers to N_2O_5 hydrolysis. These short-chain alcohols are just one of many different types of organic molecules, soluble and insoluble,[21−24]

that may coalesce within or on aerosol droplets and segregate to the surface to form mixed monolayers of widely varying porosity and reactivity.[27] We hope to extend the alcohol measurements here to soluble organic molecules with different functional groups to determine their surface activity in sulfuric acid and their ability to impede or enhance gas−liquid transport and interfacial reactions.

Acknowledgment. We are grateful to the Air Force Office of Scientific Research for supporting this work, to the Camille and Henry Dreyfus Foundation for providing a postdoctoral fellowship in environmental chemistry to S.-C.P., and to the Vilas Foundation of the University of Wisconsin. We also thank John Morris for performing early studies of N_2O_5 on bare sulfuric acid, James Krier and Casey Harris for surface tension measurements, and Steven Brown for advice on N_2O_5 synthesis. We also thank the reviewers for their valuable comments.

Appendix: Determining the Fraction of HNO_3 Remaining in Solution

We determine the fraction of N_2O_5 molecules that are converted into HNO_3 by measuring the relative flux of HNO_3 molecules that desorb from solution. Because some of the HNO_3 molecules created by hydrolysis remain behind in solution over the measurement time t_{exp}, the measured flux $I_{TD}^{HNO_3}$ in eq 2 is too small. This flux can be corrected by estimating the fraction of HNO_3 molecules that remain dissolved in the acid. The predicted thermal-desorption flux from a fresh liquid continuously exposed for a time t_{exp} is $I_{TD}^{true} = I_{enter}(1 - (erfc[(t_{exp}/\tau)^{1/2}] \cdot e^{t_{exp}/\tau})$,[66] where I_{enter} is the equivalent flux of HNO_3 entering the solution generated by the impinging N_2O_5 molecules. This flux depends on the characteristic residence time τ of the HNO_3 molecules in solution. It is given by $\tau = D(4H^*RT/\alpha_{th}\langle\upsilon\rangle)^2$, where H^* is the overall solubility of HNO_3 in M atm^{-1}, D is the HNO_3 diffusion constant, α_{th} is the HNO_3 entry probability averaged over a Boltzmann distribution of collision energies at temperature T, and $\langle\upsilon\rangle$ is the thermal velocity of HNO_3. Over the time $t = 0$ to τ, the desorption flux rises from 0 to 57% of the flux entering solution. We use the values $H^* = 2 \times 10^6$ M atm^{-1} for HNO_3 in 72 wt % H_2SO_4 at 216 K from ref 43, $D = 7 \times 10^{-9}$ cm^2 s^{-1} from ref 42, and $\alpha_{th} = 1$ from ref 53 to obtain $\tau = 0.2$ s.

The fraction f_{remain} of HNO_3 molecules that accumulate within the acid over the time t_{exp} is given by eq 8c in ref 67, where it is also graphed:

$$f_{remain}(t_{exp}) = \frac{I_{enter}t_{exp} - \int_0^{t_{exp}} I_{TD}^{true}\,dt}{I_{enter}t_{exp}} = (\tau/t_{exp})\{erfc[(t_{exp}/\tau)^{1/2}]\, e^{t_{exp}/\tau} + 2(t_{exp}/\pi\tau)^{1/2} - 1)\} \quad \text{(A.1)}$$

For $t_{exp} = 6$ s and $\tau = 0.2$ s, f_{remain} is 0.18, indicating that 18% of the HNO_3 molecules remain in the acid even over times much longer than τ. In this case, I_{TD}^{diff} should be divided by 0.82 in eq 2 to obtain the true relative flux. This correction increases f_{rxn}(bare) from 0.12 to 0.15, f_{rxn}(hexyl) from 0.05 to 0.06, and f_{rxn}(butyl) from 0.08 to 0.10 in Table 1, where the corrected quantities are labeled γ and represent our best estimates of the hydrolysis probabilities. The ratios of f_{rxn} before and after correction remain essentially unchanged, such that $\gamma_{film}/\gamma_{bare} \approx f_{rxn}(film)/f_{rxn}(bare)$.

HNO_3 desorption was also measured for a much shorter observation time of 0.27 s using a continuously rotating wheel. In this case, f_{remain} rises from 0.18 to 0.52. Despite this large correction, the final value for $\gamma(N_2O_5)$ was determined to be the same in the bare acid, 0.15 ± 0.02, suggesting that the stop−start technique may not be necessary to determine hydrolysis probabilities even when the HNO_3 product dissolves for long times.

No corrections are necessary for HCl dissolution in 72 wt % H_2SO_4 at 216 K because τ is so short ($\tau = 2 \times 10^{-4}$ and $f_{remain} = 0.03$). HBr dissolves for longer times in the bare acid ($\tau = 0.002$ s and $f_{remain} = 0.09$), but again drops to 2×10^{-4} s in the alkyl-coated acids because $\alpha \approx f_{exch}$ is larger. The value for HBr entering the bare acid in Table 1 has been corrected for a 10% increase due to HBr molecules accumulating in solution over the 0.27 s exposure and observation time.

References and Notes

(1) Finlayson-Pitts, B. J.; Pitts, J. N. *Chemistry of the Upper and Lower Atmosphere*; Academic Press: New York, 2000; Chapters 9.C and 12.C.
(2) Solomon, S. *Rev. Geophys.* **1999**, *37*, 275.
(3) Hanson, D. R.; Lovejoy, E. R. *J. Phys. Chem.* **1996**, *100*, 6397.
(4) Jacob, D. *Atmos. Environ.* **2000**, *34*, 2131.
(5) Rodriguez, J. M.; Ko, M. K. W.; Sze, N. D. *Nature* **1991**, *352*, 134.
(6) Hanson, D. R.; Ravishankara, A. R.; Solomon, S. *J. Geophys. Res. Atmos.* **1994**, *99*, 3615.
(7) Wennberg, P. O.; Cohen, R. C.; Stimpfle, R. M.; Koplow, J. P.; Anderson, J. G.; Salawitch, R. J.; Fahey, D. W.; Woodbridge, E. L.; Keim, E. R.; Gao, R. S.; Webster, C. R.; May, R. D.; Toohey, D. W.; Avallone, L. M.; Proffitt, M. H.; Loewenstein, M.; Podolske, J. R.; Chan, K. R.; Wofsy, S. C. *Science* **1994**, *266*, 398.
(8) Fahey, D. W.; Kawa, S. R.; Woodbridge, E. L.; Tin, P.; Wilson, J. C.; Jonsson, H. H.; Dye, J. E.; Baumgardner, D.; Borrmann, S.; Toohey, D. W.; Avallone, L. M.; Proffitt, M. H.; Margitan, J.; Loewenstein, M.; Podolske, J. R.; Salawitch, R. J.; Wofsy, S. C.; Ko, M. K. W.; Anderson, D. E.; Schoeberl, M. R.; Chan, K. R. *Nature* **1993**, *363*, 509.
(9) Hendricks, J.; Lippert, E.; Petry, H.; Ebel, A. *J. Geophys. Res. Atmos.* **1999**, *104*, 5531.
(10) See, for example, Badger, C. L.; Griffiths, P. T.; George, I.; Abbatt, J. P. D.; Cox, R. A. *J. Phys. Chem. A* **2006**, *110*, 6986 and ref 19.
(11) Dentener, F. J.; Crutzen, P. J. *J. Geophys. Res. Atmos.* **1993**, *98*, 7149.
(12) Tie, X.; Emmons, L.; Horowitz, L.; Brasseur, G.; Ridley, B.; Atlas, E.; Stround, C.; Hess, P.; Klonecki, A.; Madronich, S.; Talbot, R.; Dibb, J. *J. Geophys. Res.* **2003**, *108*, 8364.
(13) Evans, M. J.; Jacob, D. J. *Geophys. Res. Lett.* **2005**, *32*, L09813.
(14) Hanson, D. R.; Ravishankara, A. R. *J. Geophys. Res. Atmos.* **1991**, *96*, 17307.
(15) Zhang, R. Y.; Leu, M. T.; Keyser, L. F. *Geophys. Res. Lett.* **1995**, *22*, 1493.
(16) Fried, A.; Henry, B. E.; Calvert, J. G.; Mozurkewich, M. *J. Geophys. Res. Atmos.* **1994**, *99*, 3517.
(17) Robinson, G. N.; Worsnop, D. R.; Jayne, J. T.; Kolb, C. E.; Davidovits, P. *J. Geophys. Res. Atmos.* **1997**, *102*, 3583.
(18) Williams, L. R.; Manion, J. A.; Golden, D. M.; Tolbert, M. A. *J. Appl. Meteorol.* **1994**, *33*, 785.
(19) Kane, S. M.; Caloz, F.; Leu, M.-T. *J. Phys. Chem. A* **2001**, *105*, 6465.
(20) Murphy, D. M.; Thomson, D. S.; Mahoney, T. M. J. *Science* **1998**, *282*, 1664.
(21) Singh, H.; Chen, Y.; Tabazadeh, A.; Fukui, Y.; Bey, I.; Yantosca, R.; Jacob, D.; Arnold, F.; Wohlfrom, K.; Atlas, E.; Flocke, F.; Blake, D.; Blake, N.; Heikes, B.; Snow, J.; Talbot, R.; Gregory, G.; Sachse, G.; Vay, S.; Kondo, Y. *J. Geophys. Res. Atmos.* **2000**, *105*, 3795.
(22) Singh, H.; Chen, Y.; Staudt, A.; Jacob, D.; Blake, D.; Heikes, B.; Snow, J. *Nature* **2001**, *410*, 1078.
(23) Apel, E. C.; Hills, A. J.; Lueb, R.; Zindel, S.; Eisele, S. *J. Geophys. Res.* **2003**, *108*, 8794.
(24) Tervahattu, H.; Juhanoja, J.; Vaida, V.; Tuck, A. F.; Niemi, J. V.; Kupiainen, K.; Kulmala, M.; Vehkamaki, H. *J. Geophys. Res. Atmos.* **2005**, *110*, D06207.
(25) Brown, S. S.; Ryerson, T. B.; Wollny, A. G.; Brock, C. A.; Peltier, R.; Sullivan, A. P.; Weber, R. J.; Dube, W. P.; Trainer, M.; Meagher, J. F.; Fehsenfeld, F. C.; Ravishankara, A. R. *Science* **2006**, *311*, 67.
(26) Barnes, G. T. *Colloids Surf. A.* **1997**, *126*, 149.
(27) Gilman, J. B.; Vaida, V. *J. Chem. Phys. A* **2006**, *110*, 7581.

(28) For a review of gas transport through surfactant films, see the introduction of ref 39.
(29) Mmereki, B. T.; Chaudhuri, S. R.; Donaldson, D. J. *J. Phys. Chem. A* **2003**, *107*, 2264.
(30) Clifford, D.; Bartels-Rausch, T.; Donaldson, D. J. *Phys. Chem. Chem. Phys.* **2007**, *9*, 1362.
(31) Thornton, J. A.; Abbatt, J. P. D. *J. Phys. Chem. A* **2005**, *109*, 10004.
(32) McNeill, V. F.; Patterson, J.; Wolfe, G. M.; Thornton, J. A. *Atmos. Chem. Phys.* **2006**, *6*, 1635.
(33) Folkers, M.; Mentel, T. F.; Wahner, A. *Geophys. Res. Lett.* **2003**, *30*, 1644.
(34) Anttila, T.; Kiendler-Scharr, A.; Tillman, R.; Mentel, T. F. *J. Phys. Chem. A* **2006**, *110*, 10435.
(35) Chen, B.; Siepmann, J. I.; Klein, M. L. *J. Am. Chem. Soc.* **2002**, *124*, 12232.
(36) Daiguji, H. *J. Chem. Phys.* **2001**, *115*, 1538.
(37) Lawrence, J. R.; Glass, S. V.; Park, S.-C.; Nathanson, G. M. *J. Phys. Chem. A* **2005**, *109*, 7458.
(38) Glass, S. V.; Park, S.-C.; Nathanson, G. M. *J. Phys. Chem. A* **2006**, *110*, 7593.
(39) Lawrence, J. R.; Glass, S. V.; Nathanson, G. M. *J. Phys. Chem. A* **2005**, *109*, 7449.
(40) Torn, R. D.; Nathanson, G. M. *J. Phys. Chem. B* **2002**, *106*, 8064.
(41) Williams, G.; Clark, D. J. *J. Chem. Soc.* **1956**, 1304.
(42) Williams, L. R.; Long, F. S. *J. Phys. Chem.* **1995**, *99*, 3748.
(43) Carslaw, K. S.; Clegg, S. L.; Brimblecombe, P. *J. Phys. Chem.* **1995**, *99*, 11557. Carslaw, K. S.; Peter, T.; Clegg, S. L. *Rev. Geophys.* **1997**, *35*, 125. Calculations were performed at mae.ucdavis.edu/wexler/aim.htm.
(44) Davidson, J. A.; Viggiano, A. A.; Howard, C. J.; Dotan, I.; Fehsenfeld, F. C.; Albritton, D. L.; Ferguson, E. E. *J. Chem. Phys.* **1978**, *68*, 2085.
(45) Lowry, T. M.; Lemon, J. T. *J. Chem. Soc.* **1935**, 692.
(46) *Handbook of Chemistry and Physics*; Linde, D. R., Ed.; CRC Press: New York, 2001; Section 6, p 69.
(47) Antony, B. K.; Joshipura, K. N.; Mason, N. J. *Int. J. Mass Spectrom.* **2004**, *233*, 207.
(48) O'Connor, C. S. S.; Jones, N. C.; O'Neale, K.; Price, S. D. *Int. J. Mass Spectrom.* **1996**, *154*, 203.
(49) Jimenez, J. L.; Jayne, J. T.; Shi, Q.; Kolb, C. E.; Worsnop, D. R.; Yourshaw, I.; Seinfeld, J. H.; Flagan, R. C.; Zhang, X.; Smith, K. A.; Morris, J. W.; Davidovits, P. *J. Geophys. Res.* **2003**, *108*, 13.
(50) O'Connor, C. S. S.; Jones, N. C.; Price, S. D. *Int. J. Mass Spectrom.* **1997**, *163*, 131.
(51) Schmeling, T.; Strey, R. *Phys. Chem. Chem. Phys.* **1983**, *87*, 871.
(52) Michelson, R. R.; Staton, S. J. R.; Iraci, L. T. *J. Chem. Phys. A* **2006**, *110*, 6711.
(53) Morris, J. M.; Behr, P.; Antman, M. D.; Ringeisen, B. R.; Splan, J.; Nathanson, G. M. *J. Phys. Chem. A* **2000**, *104*, 6738.
(54) Krier, J. M.; Nathanson, G. M., to be submitted for publication.
(55) Fraser, R. T. M.; Paul, N. C. *J. Chem. Soc. B* **1968**, 659.
(56) Tikhonov, A. M.; Pingali, S. V.; Schlossman, M. L. *J. Chem. Phys.* **2004**, *120*, 11822.
(57) Hallquist, M.; Stewart, D. J.; Baker, J.; Cox, R. A. *J. Phys. Chem. A* **2000**, *104*, 3984.
(58) Li, Z. X.; Lu, J. R.; Thomas, R. K.; Rennie, A. R.; Penfold, J. *J. Chem. Soc., Faraday Trans.* **1996**, *92*, 565.
(59) Van Loon, L. L; Minor, R. N; Allen, H. C. *J. Phys. Chem. A* **2007**, submitted for publication.
(60) Hanson, D. R. *J. Phys. Chem. B* **1997**, *101*, 4998.
(61) See ref 31 for a similar resistor-model analysis of N_2O_5 hydrolysis in sea salt aerosol coated with hexanoic acid.
(62) A more polarizable solute might be expected to be more soluble in the alkyl film and therefore move through it more easily. The polarizabilities of N_2O_5 and CF_3CH_2OH, however, are estimated to be 8 and 5 Å^3, respectively, in the opposite order of their apparent mobility. This observation led us to focus on the OH group rather than the CF_3CH_2 group as a facilitator of the permeation of CF_3CH_2OH. Our measurements also indicate that H_2O moves without resistance through the hexyl and butyl films. For polarizability estimates, see Miller, K. A.; Savchik, J. A. *J. Am. Chem. Soc.* **1979**, *101*, 7206, and Wincel, H; Mereand, E; Castleman, A. W. *J. Phys. Chem.* **1995**, *99*, 1792.
(63) Hanson, D. R.; Lovejoy, E. R. *Geophys. Res. Lett.* **1994**, *21*, 2401.
(64) The average diffusion depth over a time $\tau/2$ is estimated by calculating $\langle z(t)\rangle = [\int c(z,t)\,dz]/[\int c(z,t)\,dz] = 0.80(Dt)^{1/2}$, where $c(z,t)$ is the concentration profile of the gas in the liquid for initial exposure at $t = 0$. This profile is $c(z,t)/c(t \rightarrow \infty) = \mathrm{erfc}(z/(4Dt)^{1/2}) - \exp(z/(D\tau))^{1/2}\exp(t/\tau)\mathrm{erfc}((t/\tau)^{1/2} + z/(4Dt)^{1/2})$. For a total residence time of τ and diffusion in one direction of time $t = \tau/2$, $\langle z(\tau/2)\rangle \approx 0.6(D\tau)^{1/2}$. This profile is obtained from the diffusion equation and the boundary condition $-D\partial c(z,t)/\partial z|_{z=0} = (D/\tau)^{1/2}(c(t \rightarrow \infty) - c(z,t))$. See also the Appendix of ref 66 and page 72 of Carslaw, H. S; Yaeger, J. C. *Conduction of Heat in Solids*; Oxford University Press; Oxford, 1959.
(65) Singh, H. B.; Salas, L. J.; Chatfield, R. B.; Czech, E.; Fried, A.; Walega, J.; Evans, M. J.; Field, B. D.; Jacob, D. J.; Blake, D.; Heikes, B.; Talbot, R.; Sachse, G.; Crawford, J. H.; Avery, M. A.; Sandholm, S.; Fuelberg, H. *J. Geophys. Res.* **2004**, *109*, D15S07.
(66) Hanson, D. R.; Ravishankara, A. R. *J. Phys. Chem.* **1993**, *97*, 12309.
(67) Robinson, G. N.; Worsnop, D. R.; Jayne, J. T.; Kolb, C. E.; Swartz, E.; Davidovits, P. *J. Geophys. Res. Atmos.* **1998**, *103*, 25371.